Iran Polym J (2014) 23:531–545
DOI 10.1007/s13726-014-0248-5

ORIGINAL PAPER

High-performance polymer/nanodiamond composites: synthesis and properties

Rozina Ashraf · Ayesha Kausar · Muhammad Siddiq

Received: 6 November 2013 / Accepted: 20 April 2014 / Published online: 8 May 2014

Abstract Conjugated polymer/nanodiamond nanocomposites have been known as high-performance materials due to improved physical properties relative to conventional composites. In this attempt, novel conjugated polymer/nanodiamond nanocomposites were successfully prepared by in situ oxidative polymerization. Physical characteristics of the resultant nanocomposites were explored using Fourier transform infrared spectroscopy, field emission scanning electron microscope (FESEM), energy dispersive X-ray spectroscope, differential scanning calorimeter, thermogravimetric analysis and X-ray diffraction spectroscopy. Structural analysis revealed the oxidative polymerization of various matrices [polyaniline (PANi), polypyrrole (PPy), polythiophene (PTh) and polyazopyridine (PAP)] over the surface of functionalized (F-NDs) and non-functionalized nanodiamonds (NF-NDs) thus ensuing NF-NDs/PAP/PANi/PPy, F-NDs/PAP/PANi/PPy, NF-NDs/PANi/PPy/PTh and F-NDs/PANi/PPy/PTh nanocomposites. FESEM images depicted the fibrillar morphology of resulting nanocomposites with granular arrangement of nanofiller in matrix. Thermal analysis results showed that the functionalized F-NDs/PAP/PANi/PPy hybrid had higher value of 10 % weight loss around 489 °C relative to F-NDs/PANi/PPy/PTh with T_{10} at 471 °C. The glass transition temperature was found to be 99 and 105 °C for NF-NDs/PANi/PPy/PTh and F-NDs/PANi/PPy/PTh, respectively. On the other hand, NF-NDS/PAP/PANi/PPy and F-NDs/PAP/PANi/PPy showed higher T_g's of 109 and 118 °C. The conductivity of NF-NDs/PAP/PANi/PPy was 3.8 Scm^{-1} and improved with the functionalized filler loading in F-NDs/PAP/PANi/PPy up to 5.4 Scm^{-1}, while NF-NDs/PANi/PPy/PTh and F-NDs/PANi/PPy/PTh had relatively lower values around 2.9 and 3.7 Scm^{-1}, respectively. New conducting nanocomposites may act as useful contenders in significant industrial applications such as polymer Li-ion battery.

Keywords Multi-layered nanocomposite · Conductivity · Nanodiamonds · Fibrillar morphology

R. Ashraf · A. Kausar
Nanosciences and Catalysis Division, National Centre For Physics, Quaid-i-Azam University Campus, Islamabad 44000, Pakistan

R. Ashraf · M. Siddiq (✉)
Department of Chemistry, Quaid-i-Azam University, Islamabad, Pakistan
e-mail: m_sidiq12@yahoo.com

Introduction

Nanomaterials have gained tremendous interest of scientists and researchers owing to improved properties of these kinds of materials relative to the bulk materials [1, 2]. Among carbon-based nanomaterials, fullerene, carbon nanotube, nanodiamond and graphene have been widely exploited.

One of the most important forms of carbon nanostructure family is the nanodiamonds (NDs). In recent decades, nanodiamond powder (usually obtained through the detonation of carbon-based explosives) has attracted exceptional research concern [3, 4]. Nanodiamond powder has the fine combination of properties such as chemical stability, hardness, crytsallinity, dopability, and low toxicity [5, 6]. Moreover, nanodiamonds have narrow particle size distribution (typically 4–6 nm), small diameter (~5 nm), large surface area (300–500 m^2/g), and superior thermal conductivity, optical and electrical properties [7–9]. Due to the above-mentioned properties, nanodiamond has vast

potential as adsorbents, reinforcement of plastics and resins, colloidal suspension, microabrassive, refrigerating fluids, quantum dots, etc. Polymer-based nanocomposites have made tremendous breakthroughs in advanced functionalized materials such as rechargeable batteries, super capacitors, electronic devices, sensors and functional electrodes [10–12]. These applications have been attributed to remarkable improvement in thermal, electrical and mechanical properties of polymers by incorporation of small amount of nanofiller [13–15]. Preparation of layered nanocomposites has been an interesting research field. However, such type of nanocomposites depicts poor electrical and thermal conductivity [16, 17]. To overcome these impediments, carbon-based nanomaterials including graphite, carbon black, carbon nanotube and nanodiamonds have been used as reinforcement [18–20].

Among carbon-based nanomaterials, spherical nanoparticles have received significant interest due to their highest surface-to-volume ratio [21–23]. Consequently, nanodiamonds have been known as popular reinforcement due to nearly spherical shape, nano-size, and exceptional physiochemical and mechanical characteristics [24–27]. In this regard, π-conjugated or conducting polymers have been known as significant materials due to tunable electronic and physical, mechanical and optical characteristics. These polymers are, thus, widely applicable in batteries, electrochromic devices, anti-corrosion coatings, photovoltaics, organic transistors and light emitting diodes [28, 29]. Polyaniline, polythiophene, polypyrrole, etc. are among the most commonly used conducting organic polymers. Accordingly, these conducting organic polymers in combination with NDs exhibit remarkable mechanical, thermal and electrical characteristics.

In recent times, major research focus has been the utilization of cheaper, efficient and non-contaminating energy resources. One of the attractive ways to resolve the intrinsic problem is the use of Li-ion batteries which convert chemical energy into electrical energy through chemical bond cleavage. Ionically conducting gel polymer electrolyte (GPE) has been considered as an excellent choice for the replacement of liquid electrolyte due to flexible characteristics, good cyclability, safety, energy density, etc. [30]. New layered polymer/nanodiamond nanocomposite (electrolyte) having fine mechanical and electrical characteristics plus resistance toward environmental exposition may be used in rechargeable polymer lithium ion batteries [31].

In this report, we have opted chemical oxidative in situ polymerization route for the synthesis of functionalized (F-NDs) and non-functionalized nanodiamonds (NF-NDs)-based nanocomposites using polyaniline (PANi), polypyrrole (PPy), polythiophene (PTh) and polyazopyridine (PAP) as layered matrices. NF-NDs/PAP/PANi/PPy, F-NDs/PAP/PANi/PPy, NF-NDs/PANi/PPy/PTh and F-NDs/PANi/PPy/PTh nanocomposites were fabricated by in situ polymerization of monomers (2,6-diamino pyridine, aniline, thiophene and pyrrole) over the nanodiamond surface. To the best of our knowledge, core shell NDs/PAP/PANi/PPy was first time chemically synthesized through this route. Furthermore, physical characteristics of the prepared nanocomposites were explored using suitable techniques. The aim of this study was to synthesize nanocomposite with better electrical conductivity without decreasing the thermal properties.

Experimental

Materials

Nanodiamonds synthesized by detonation route with 99 % purity and size of clusters 64–120 nm were adopted. 2,6-Diaminopyridine (98 %), aniline (99 %), pyrrole (98 %), thiophene (>99 %) were purchased from Aldrich and kept at 0 °C prior to use. Various other reagents such as potassium dichromate ($K_2Cr_2O_7$, 99.99 %), anhydrous iron (III) chloride ($FeCl_3$, >98 %), sulfuric acid (H_2SO_4, 98 %), hydrochloric acid (HCl, 37 %), nitric acid (HNO_3, 70 %), sodium hydroxide (NaOH, >98 %) and sodium nitrite ($NaNO_2$, >97 %) were also procured from Aldrich and used as received.

Measurements

Infrared (IR) spectra were recorded using a FTSW 300 MX, Bio-Rad (USA) Fourier transform infrared (FTIR) spectrometer (4 cm^{-1} resolution). Field emission scanning electron microscopy (FESEM) of samples was performed using a JSM5910, JEOL (Japan) microscope. Thermal stability was verified by a Mettler Toledo TGA/SDTA 851 (Switzerland) thermogravimetric analyzer using 1–5 mg of the sample in Al_2O_3 crucible at a heating rate of 10 °C min^{-1}. Differential scanning calorimetry (DSC) was performed by a Mettler Toledo DSC 822 (Switzerland) differential scanning calorimeter taking 5–10 mg of samples in aluminum pans and heated at a rate of 10 C min^{-1}. X-ray diffraction patterns were obtained at room temperature on an X-ray diffractometer (PW 3040/60 X'pert PRO, PANalytical, The Netherland) using Ni-filtered Cu Kα radiation (40 kV, 30 mA). An Energy dispersive X-ray (EDX) spectrometer (EDX-720/800HS/900HS, Shimadzu Europe, Germany) was also used for elemental analysis. Electrical conductivity was measured using a Keithley 614 electrometer (USA) and the four-probe method.

Scheme 1 Functionalization of nanodiamonds

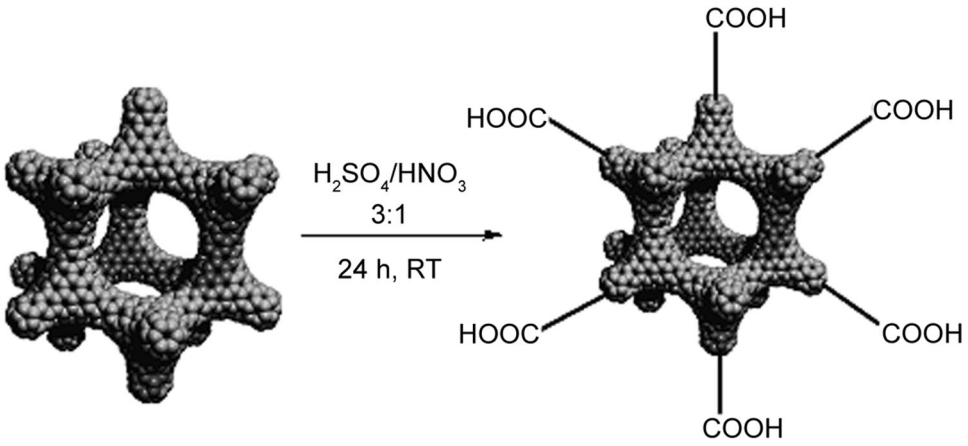

Purification of nanodiamonds

In nanodiamonds synthesis, various impurities were incorporated in nanodiamond particulates hindering their applications. Essentially, removal of these impurities for example sp^2 carbon species (graphite, amorphous carbon, fullerene like carbon and some hetero atoms) and incombustible residues (metals and oxides, 1–8 wt%) by thermal oxidation and acid treatment (using liquid oxidants such as HNO_3, mixture of H_2SO_4 and HNO_3, $K_2Cr_2O_7$ in H_2SO_4, KOH/KNO_3, Na_2O_2, and HNO_3/H_2O_2 under pressure of $HClO_4$) has been prerequisite for further appliance of nanodiamonds. To get rid of sp^2 nondiamond by product from the detonation soot, as-prepared diamond soot was subjected to thermal oxidation in conc. HNO_3 at 200–250 °C and 80–100 atm pressure in a titanium alloy reactor. Further purification was performed using HCl treatment (80–100 °C) followed by repeated washing with deionized water until pH 7 was attained [32, 33].

Functionalization of nanodiamonds

Introduction of discrete functional groups on the filler surface was adopted to modify the nanodiamond characteristics. Among various functionalized nanodiamonds, carboxylated nanodiamonds have been more conveniently synthesized. Surface functionalization of purified nanodiamonds was carried out in a mixture of strong acids, i.e., H_2SO_4 and HNO_3 (3:1, respectively) at 30 °C with continuous magnetic stirring of 24 h. The above mixture was poured into a beaker containing 200 mL hot water (70 °C) and stirred for 10 h (room temperature). After filtration, products were washed several times with deionized water and dried at 80 °C for 4 h (Scheme 1).

Synthesis of NF-NDs/PANi/PPy/PTh

In 250 mL round bottom flask, 0.5 mL aniline was dispersed in 50 mL aqueous HCl and stirred for 1 h. A sample of 0.1 g purified nanodiamonds were dispersed in the above mixture and again stirred for 12 h resulting in adsorption of aniline monomer on the nanodiamonds surface. To the above mixture, 50 mL $K_2Cr_2O_7$/HCl solution [0.5 g $K_2Cr_2O_7$ in 0.1 M aqueous HCl (50 mL)] was added dropwise at 0 °C for 6 h (labeled as **A**). Secondly, a mixture of 0.5 mL pyrrole and aqueous HCl (50 mL) was prepared separately and added dropwise to **A** and further agitated for 12 h. To initiate the polymerization of pyrrole, a solution of $FeCl_3$ (1.2 g) in 0.1 M HCl (50 mL) was added dropwise to the above mixture at 0 °C for 6 h (labeled as **B**). A solution of 0.5 mL thiophene in 50 mL aqueous HCl (0.1 M) was added dropwise to **B**. Further stirring for 12 h was prerequisite for the adsorption of monomers. Polymerization was facilitated by the addition of a solution of $FeCl_3$ (1.2 g) in 0.1 M HCl (50 mL) at 0 °C. The product obtained was washed with deionized water and dried at 70 °C.

Synthesis of F-NDs/PANi/PPy/PTh

In the synthesis of core shell F-NDs/PANi/PPy/PTh constituting F-NDs (functionalized nanodiamonds) the same synthetic route was opted as depicted in Scheme 2.

Synthesis of NF-NDs/PAP/PANi/PPy

An sample of 2,6-diamino pyridine (1.09 g) was initially dissolved in H_2O/HCl (13:4 mL, respectively). In a separate beaker, 0.68 g $NaNO_2$ was dissolved in 7 mL H_2O and added dropwise to the above mixture at 0 °C

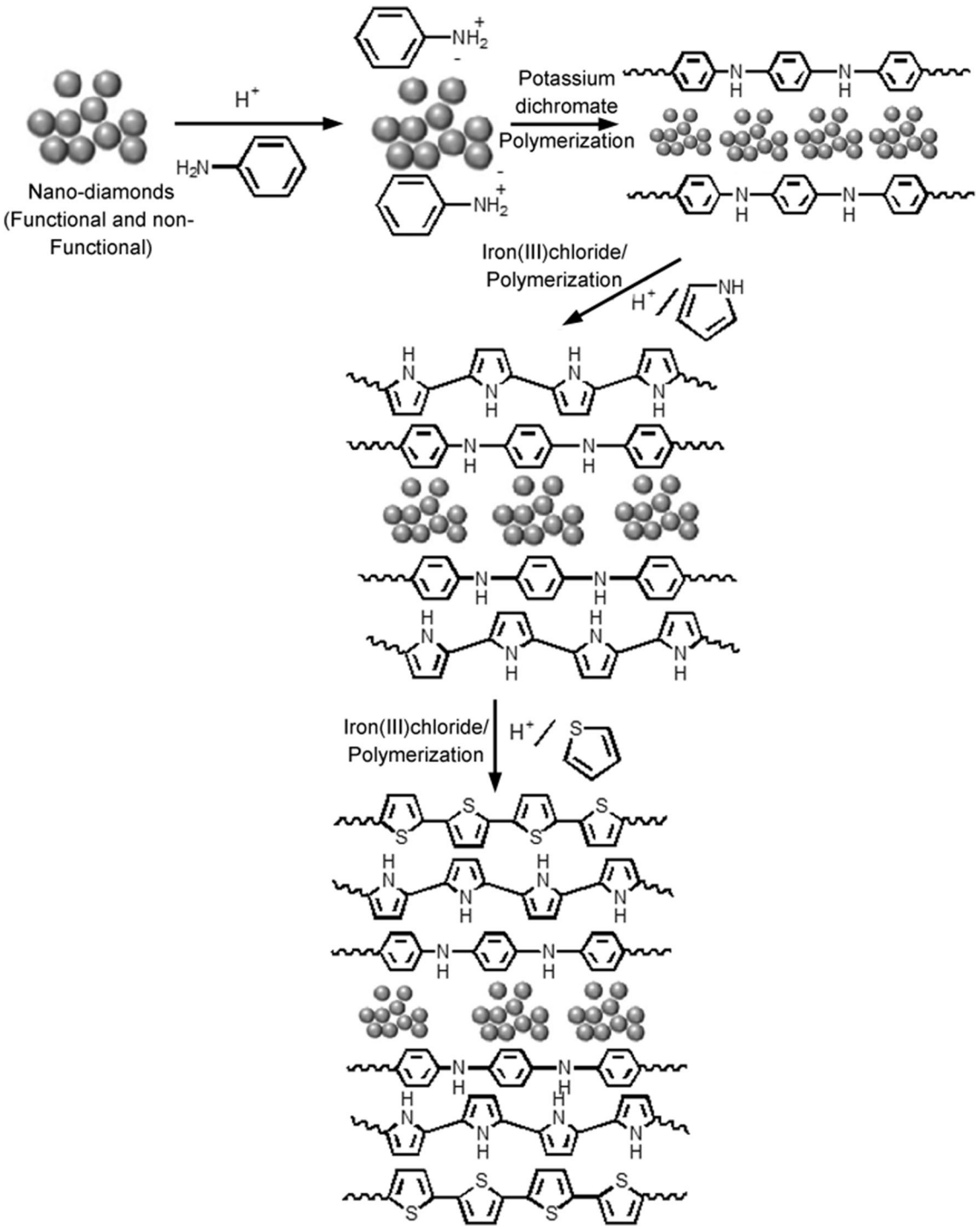

Scheme 2 Schematic synthesis of NDs/PANi/PPy/PTh nanocomposite

for 3 h (labeled as **C**). Amount of 0.1 g of NF-NDs was added to the mixture **C** and labeled as **D**. In the next step, 0.5 mL aniline was dissolved in 0.1 M HCl (50 mL) and added dropwise to **D** with continuous stirring for 12 h. The polymerization of aniline was initiated by dropwise addition of a mixture of 0.5 g $K_2Cr_2O_7$ in 0.1 M HCl (50 mL) at 0 °C for 6 h (**E**). Afterward, a solution of 0.5 mL pyrrole in 0.1 M HCl (50 mL) was prepared and added dropwise to the **E.** The dropwise addition of $FeCl_3$/HCl [1.2 g $FeCl_3$/0.1 M HCL (50 mL)] at 0 °C for 6 h initiated the polymerization of pyrrol. The resulting nanocomposite was obtained by filtration

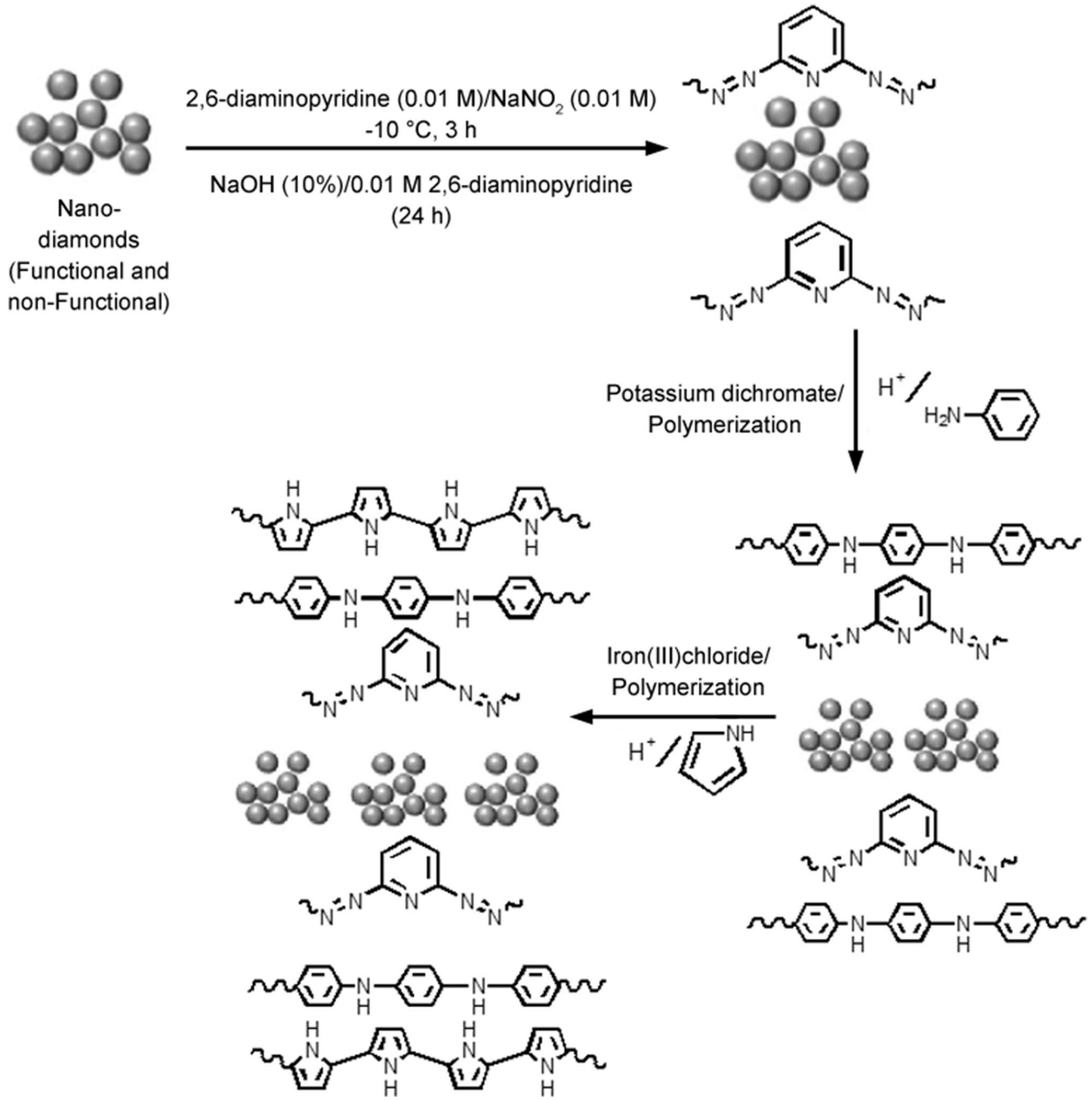

Scheme 3 Schematic representation for synthesis of NDs/PAP/PANi/PPy nanocomposite

and washed repeatedly with deionized water. Finally, the product was dried at 70 °C.

Synthesis of F-NDs/PAP/PANi/PPy

In the synthesis of F-NDs/PAP/PANi/PPy, the same procedures were adopted as illustrated in Scheme 3. The only difference was the use of functionalized nanodiamonds.

Results and discussion

Spectroscopic analysis

The structural elucidation of nanofiller and nanocomposites was carried out using FTIR (Table 1) technique. FTIR spectra of nanodiamonds (functionalized and non-functionalized) are depicted as spectra (a) and (b) in Fig. 1, respectively. The absorption bands around 3,003 and

Table 1 FTIR data of functionalized nanodiamonds, un-functionalized nanodiamonds and nanocomposites

Sample code	Aromatic C–H ν (cm^{-1})	O–H ν (cm^{-1})	C=O ν (cm^{-1})	Sec. aromatic amine ν (cm^{-1})	Thiophene ν (cm^{-1})	N=N ν (cm^{-1})	C–N ν (cm^{-1})
NF-NDs	3,001	–	–	–	–	–	–
F-NDs	3,003	3,479	1,720	–	–	–	–
NF-NDs/PANi/PPy/PTh	3,019	–	–	3,298, 1,596	1,451	–	1,255
F-NDs/PANi/PPy/PTh	3,018	3,456	1,718	3,291, 1,597	1,469	–	1,292
NF-NDs/PAP/PANi/PPy	3,003	–	–	3,324, 1,595	–	1,414	1,292
F-NDs/PAP/PANi/PPy	3,001	3,498	1,717	3,354, 1,597	–	1,413	1,298

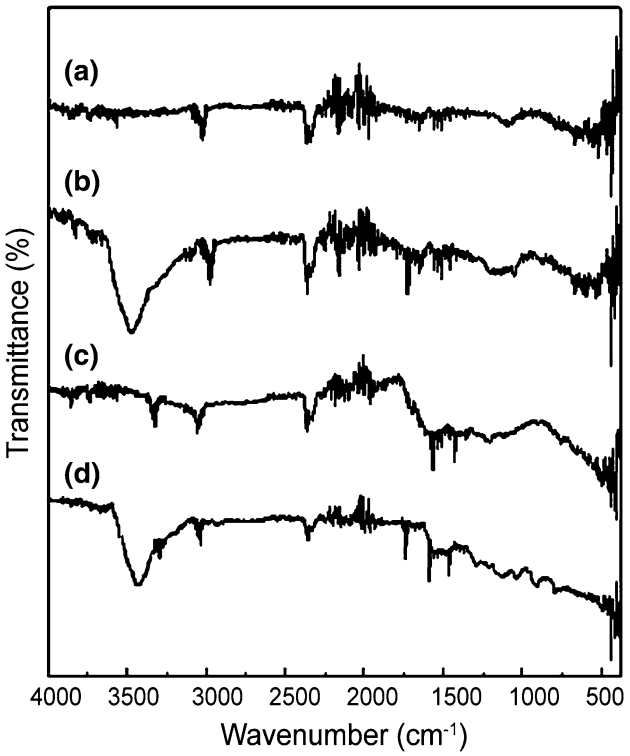

Fig. 1 FTIR spectra of *a* purified nanodiamonds, *b* functionalized nanodiamonds, *c* NF-NDs/PANi/PPy/PTh and *d* F-NDs/PANi/PPy/PTh nanocomposites

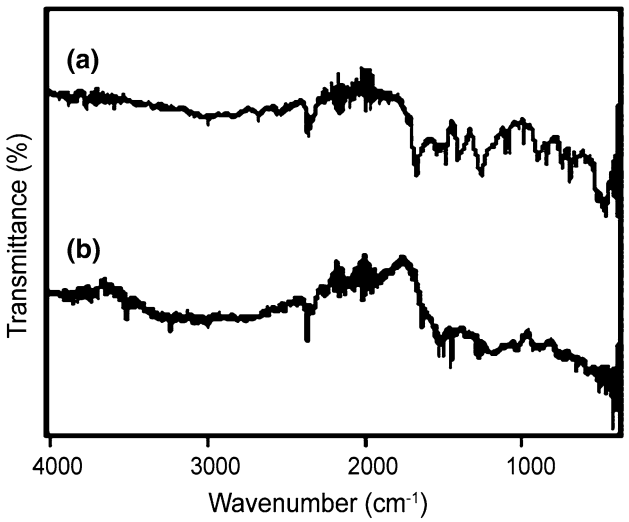

Fig. 2 FTIR spectra of *a* NF-NDs/PAP/PANi/PPy and *b* F-NDs/PAP/PANi/PPy

3,001 cm^{-1} were found due to the aromatic protons of functionalized and non-functionalized nanodiamond particles, respectively. The carboxylic acid functionalization was confirmed by the appearance of hydroxyl and carbonyl stretching vibrations at 3,479 and 1,720 cm^{-1}, respectively. Moreover, during acid functionalization there was the possibility of the introduction of SO_3H groups on the surface of nanodiamonds. Therefore, IR bands of S=O groups was found at 1,190 cm^{-1} (asymmetric stretching vibration) and in the range 1,000–1,040 cm^{-1} (symmetric stretching vibration). Aromatic C–H stretching vibration was found at 3,019 cm^{-1}, while secondary aromatic amine stretching and bending vibrations were observed at 3,298 and 1,596 cm^{-1} for NF-NDs/PANi/PPy/PTh (spectrum (c) in Fig. 1). Moreover, the absorption bands at 1,451 and 1,255 cm^{-1} were characteristics of thiophene ring vibration and C–N stretch, respectively. On the other hand, functionalized composite F-NDs/PANi/PPy/PTh [spectrum (d) in Fig. 1] demonstrated characteristics peaks at 3,456 and 1,718 cm^{-1} owing to carboxylic acid groups.

In spectrum (a) in Fig. 2, N–H stretching and bending vibrations have been appeared at 3,324 and 1,595 cm^{-1}, respectively, while characteristic absorption of N=N vibration is found at 1,414 cm^{-1} owing to the azo-based polymer in NF-NDs/PAP/PANi/PPy. Absorption peak of C–N vibration was appeared at 1,292 cm^{-1}. Similarly, F-NDs/PAP/PANi/PPy displayed nearly identical bands at 3,354, 1,597 (N–H vibrations), 1,413 (N=N bond) and 1,298 cm^{-1} (C–N vibration) as shown in spectrum (b) in Fig. 2. The stretching vibrations at 1,717 and 3,498 cm^{-1} were attributed to the acidic carbonyl and hydroxyl functionalities, respectively. Furthermore, aromatic C–H stretching vibration appeared at 3,003 and 3,001 cm^{-1} for NF-NDs/PAP/PANi/PPy and F-NDs/PAP/PANi/PPy, respectively.

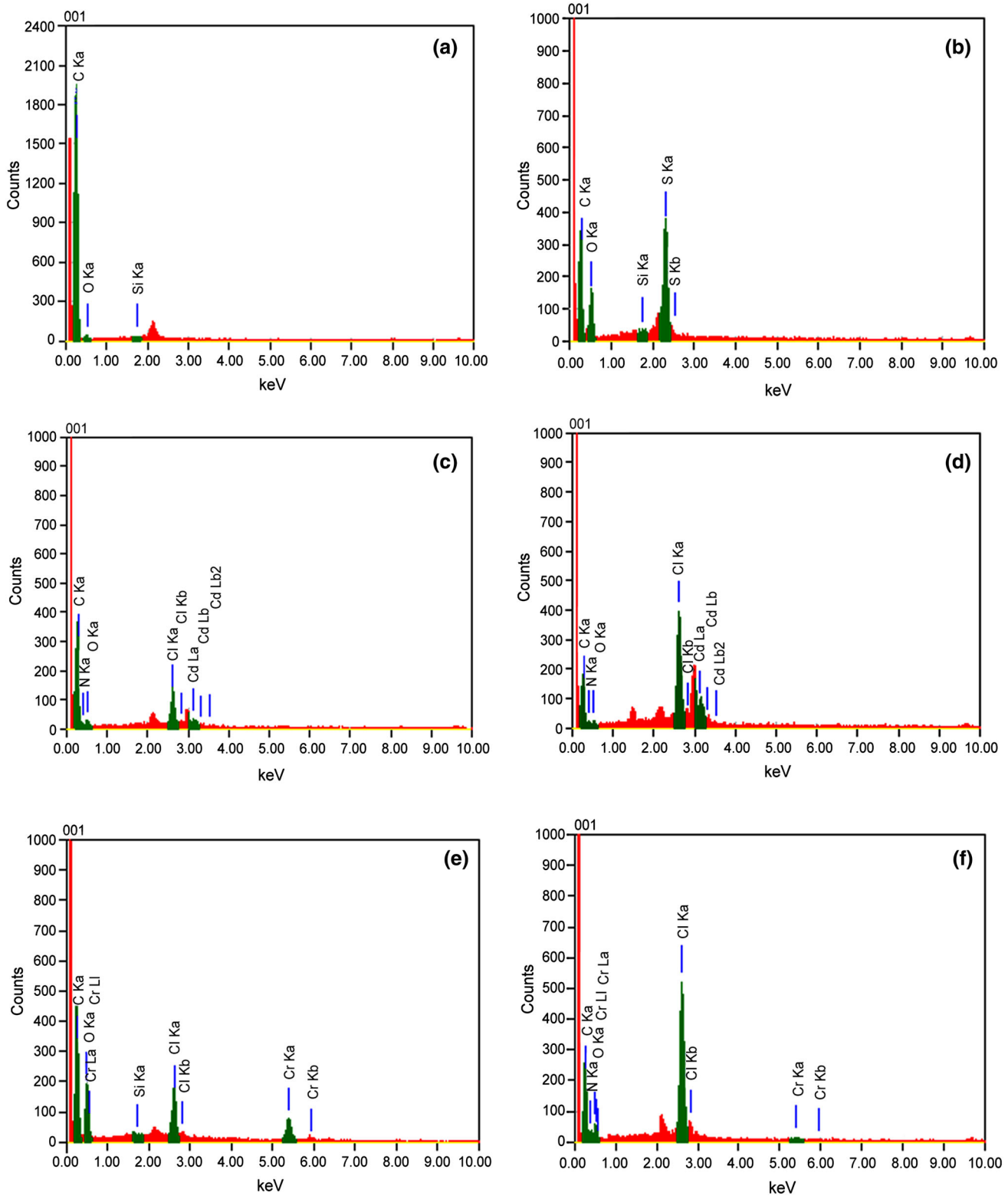

Fig. 3 EDX spectra of **a** non-functionalized nanodiamonds, **b** functionalized nanodiamonds, **c** NF-NDs/PANi/PPy/PTh, **d** F-NDs/PANi/PPy/PTh, **e** NF-NDs/PAP/PANi/PPy, and **f** F-NDs/PAP/PANi/PPy samples

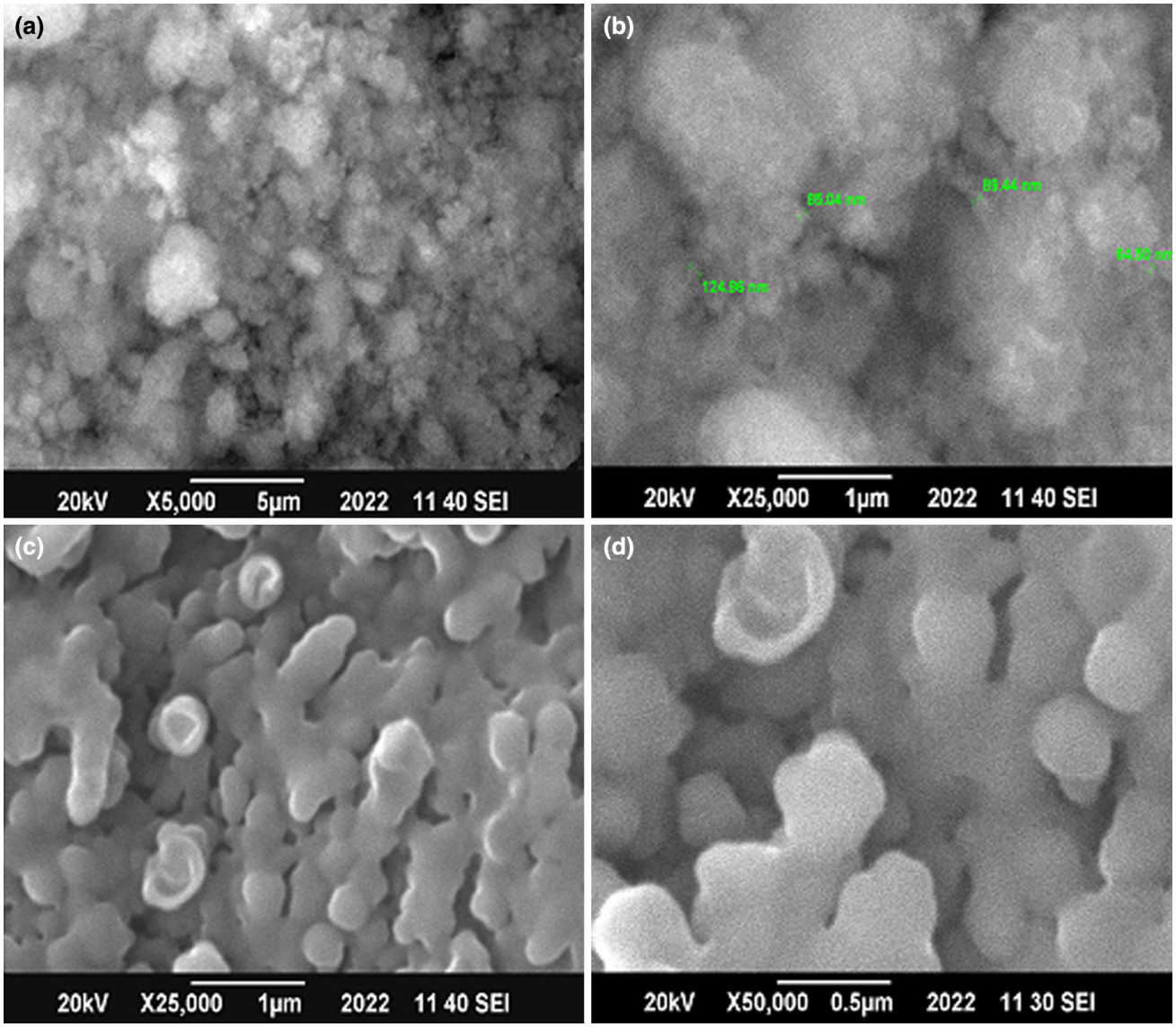

Fig. 4 FESEM micrographs of **a** non-functionalized nanodiamonds at magnification ×5,000; **b** non-functionalized nanodiamonds at magnification ×25,000; **c** functionalized nanodiamonds at magnification ×25,000; **d** functionalized nanodiamonds at magnification ×50,000

Elemental analysis

EDX analysis of nanodiamonds and nanocomposites

Energy dispersive X-ray (EDX) spectroscopy analysis was performed to investigate the composition of nanodiamonds (purified and functionalized) and nanocomposites. EDX spectra in Fig. 3a and b represent the composition of nanodiamonds and in Fig. 3c–f stand for the nanocomposites.

The spectra of purified nanodiamonds (Fig. 3a) did not show the presence of any impurity. However, the minute amount of Si was due to the catalyst used in the synthetic procedure. EDX spectrum of purified nanodiamonds shows the atomic percent of C = 90 wt%, O = 9.8 wt% and Si = 0.19 wt%. As it is appeared from Fig. 3b, the functionalized nanodiamonds had higher oxygen and lower silicon content (compared with purified nanodiamonds) in addition to carbon and sulfur traces (as impurity). The atomic percentages of functionalized nanofiller were found to be C = 64.53 wt%, Si = 0.07 wt%, O = 29.86 wt%, and S = 5.55 wt%. The amount of 5.55 wt% sulfur in functionalized nanodiamond came from the sulfuric acid treatment during functionalization. High content of sulfur in the functionalized ND was due to the introduction of SO_3H groups during the oxidative functionalization as also detected in FTIR results.

EDX spectrum of NF-NDs/PANi/PPy/PTh (Fig. 3c) shows atomic percentages of C = 43.56 wt%, N = 7.78

wt%, O = 35.19 wt%, Cl = 2.31 wt% and Cd = 0.38 wt%. The composition of non-functionalized nanocomposite is seemed to be dependent on the type of monomer and catalyst involved in the synthesis. Elemental composition confirmed the absence of impurities but small percentages of chlorine and cadmium were found.

Figure 3d shows the spectrum of F-NDs/PANi/PPy/PTh nanocomposite with C = 48.16 wt%, N = 41.10 wt%, O = 12.65 wt%, Cl = 7.78 wt% and Cd = 1.09 wt%. Higher oxygen and nitrogen content were detected in F-NDs/PANi/PPy/PTh nanocomposite relative to NF-NDs/PANi/PPy/PTh sample. The increase in nitrogen content for F-NDs/PAP/PANi/PTh was due to better layering of polymer on the functionalized filler. For NF-NDs/PAP/PANi/PPy nanocomposite (Fig. 3e), the composition was found as C = 60.73 wt%, O = 14.10 wt%, Si = 0.03 wt%, Cl = 2.55 wt% and Cr = 2.30 wt%. Traces of presented chlorine and chromium impurities may be due to the catalyst used during polymerization.

EDX spectrum of F-NDs/PAP/PANi/PPy nanocomposite (Fig. 3f) shows C = 50.26 wt%, O = 34.39 wt%, N = 29.46 wt%, Cl = 5.93 wt% and Cr = 0.24 wt%. Oxygen and chlorine atomic percentages were found to be higher in functionalized nanodiamond nanocomposite. The significant amount of nitrogen observed in this nanocomposite sample can be due to the better layering of PAP. Moreover, traces of chromium as impurity were detected.

Morphological investigation

Morphology of nanodiamonds

FESEM micrographs of nanodiamonds (Fig. 4a–d) depict the typical aggregates of purified nanodiamonds due to significant interaction among nano-sized particles and the presence of micro and nano-sized grains/nanodiamond crystals. Steady re-nucleation or polynucleation of initial nuclei resulted in the columnar morphology of microcrystalline diamond. Nanocrystalline diamonds were formed when the newly formed growth center suppressed the growth of former crystals. Nanocrystallites with smooth granular surface resembling spherical particles were thus observed.

Figure 4a and b shows larger and smaller aggregates of non-functionalized nanodiamonds, while the micrographs of functionalized nanodiamonds are presented in Fig. 4c and d, correspondingly. Morphological characterization confirmed that the nanodiamond particles possessed 90–120 nm diameters depicting their high aspect ratio. Functionalization busted the microcrystalline diamond aggregates into smaller one thus leading to homogenous dispersibility of functionalized NDs. Functionalization also created significant number of active sites (defects) on the surface without altering nanodiamond structural chemistry. Micrograph at higher resolution (Fig. 4c) depicts even dispersion, smooth and clear diamond shape of nanoparticulates.

Morphology of NDs/PAP/PANi/PTh nanocomposites

Figure 5a, b shows irregular morphology of nanocomposite comprising of non-functionalized nanodiamond particulates embedded in polymer aggregates. Morphologies of F-NDs/PANi/PPy/PTh nanocomposites, i.e., based on functionalized nanodiamonds and conducting polymers are depicted in Fig. 5c–f. Functionalized nanodiamonds having high specific surface area provided large number of sorption sites for the adsorption of monomers. Therefore, homogenous layered polymerization was facilitated due to the enhanced interaction between the external surface of functionalized nanodiamonds and the matrix. Consequently, F-NDs/PANi/PPy/PTh depicted exclusive morphology of tightly woven interconnected fibrous network (polymer) with embedded nanodiamonds (Fig. 5d, e). Besides, the nanodiamonds homogenously coated with conducting polymers formed granular arrangements on the fibrous matrix network. Such a morphological profile may offer a pathway for the transport of ions and solvent molecules within the nanocomposite and may lead to increased electrochemical characteristics.

Morphology of NDs/PAP/PANi/PPy nanocomposites

Figure 6a, b shows agglomerated and globular morphology for NF-NDs/PAP/PANi/PPy nanocomposite. Polymer agglomerates can be observed in the micrographs due to uneven adsorption of monomers over non-functionalized nanodiamond surface. Figure 6b depicts the complete covering of nanodiamonds with polymer aggregated due to non-homogenous polymerization. FESEM images of F-NDs/PAP/PANi/PPy (Fig. 6c–f) are somewhat different. The micrographs reveal comparatively even dispersion of polymer-coated nanodiamonds in F-NDs/PAP/PANi/PPy. Due to consistent polymerization of monomers on functionalized NDs surface, the diameter of nanofillers (Fig. 6c, d) was found to be larger relative to that of pure nanodiamonds.

Thermal analysis

DSC and TGA profiles of nanocomposites are showed in Figs. 7, 8, 9, 10 and their corresponding data were summarized in Table 2. The glass transition temperatures (taken as middle point of change in slope of base line in DSC thermograms) were found to be 99 and 105 °C for NF-NDs/PANi/PPy/PTh and F-NDs/PANi/PPy/PTh,

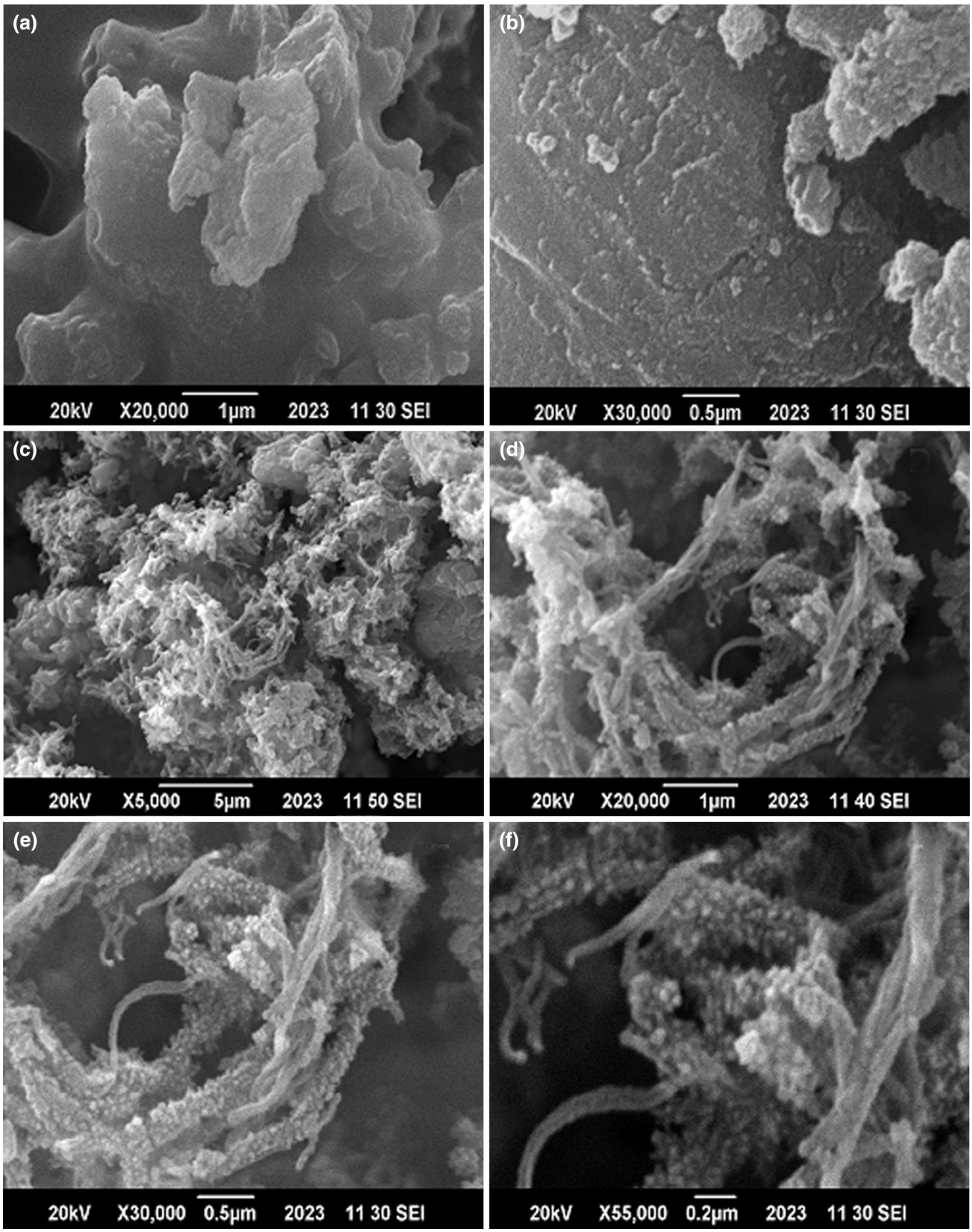

Fig. 5 FESEM micrographs of **a** NF-NDs/PANi/PPy/PTh at magnification ×20,000; **b** NF-NDs/PANi/PPy/PTh at magnification ×30,000; **c** F-NDs/PANi/PPy/PTh at magnification ×5,000; **d** F-NDs/PANi/PPy/PTh at magnification ×20,000; **e** F-NDs/PANi/PPy/PTh at magnification ×30,000; **f** F-NDs/PANi/PPy/PTh at magnification ×55,000

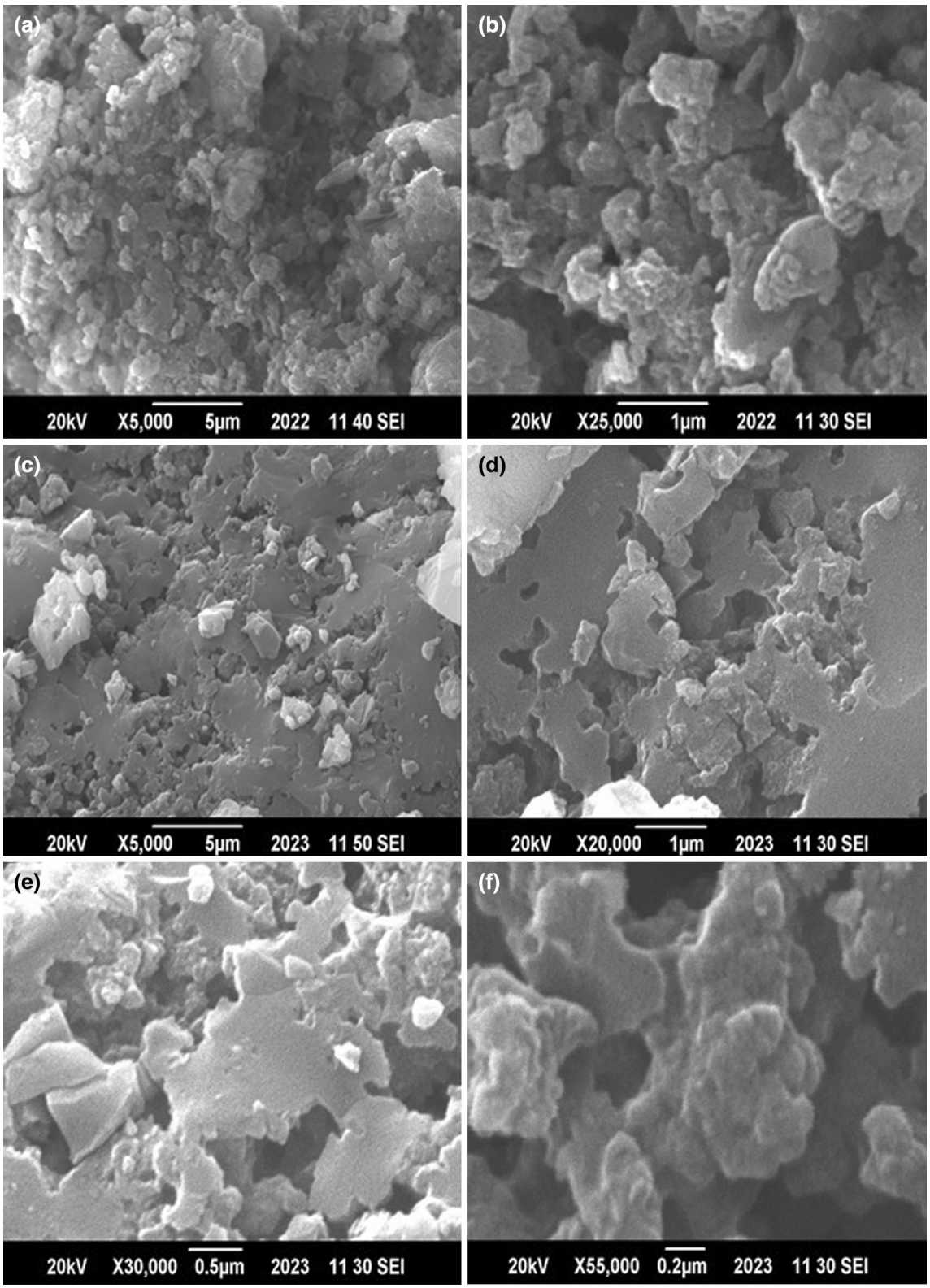

Fig. 6 FESEM micrographs of **a** NF-NDs/PAP/PANi/PPy at magnification ×5,000; **b** NF-NDs/PAP/PANi/PPy at magnification ×25,000; **c** F-NDs/PAP/PANi/PPy at magnification ×5,000; **d** F-NDs/PAP/PANi/PPy at magnification ×20,000; **e** F-NDs/PAP/PANi/PPy at magnification ×30,000; **f** F-NDs/PAP/PANi/PPy at magnification ×55,000

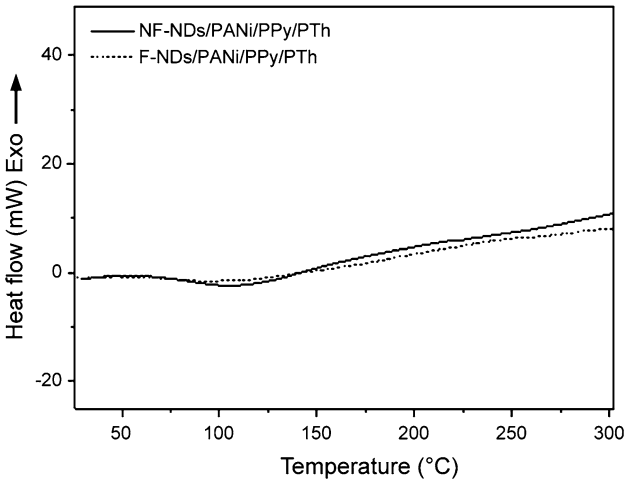

Fig. 7 DSC thermograms of NDs/PANi/PPy/PTh at heating rate of 10 °C min^{-1} in N_2

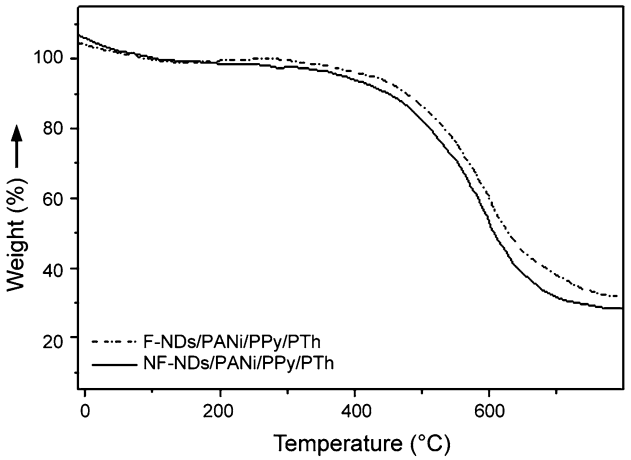

Fig. 9 TGA thermograms of NDs/PANi/PPy/PTh at heating rate of 10 °C min^{-1} in N_2

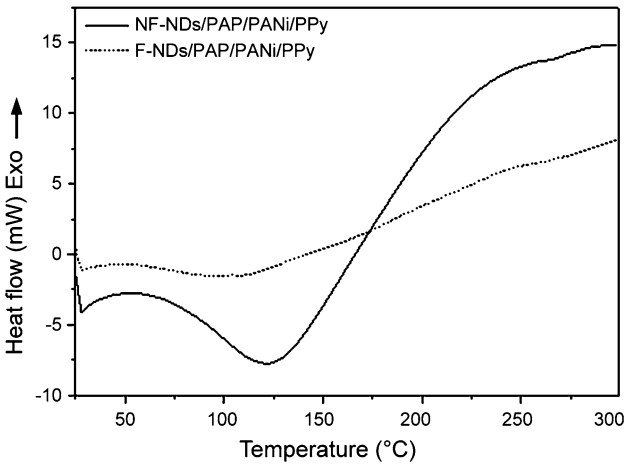

Fig. 8 DSC thermograms of NDs/PAP/PANi/PPy at heating rate of 10 °C min^{-1} in N_2

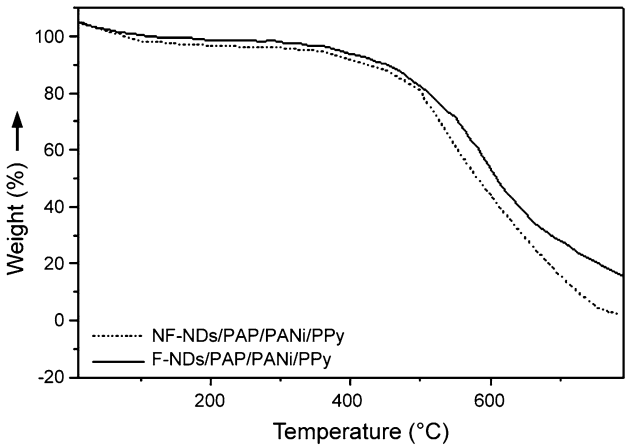

Fig. 10 TGA thermograms of NDs/PAP/PANi/PPy at heating rate of 10 °C min^{-1} in N_2

respectively (Fig. 7). On the other hand, NF-NDs/PAP/PANi/PPy and F-NDs/PAP/PANi/PPy showed higher T_g's of 109 and 118 °C, respectively (Fig. 8). The increase in glass transition temperature was due to the incorporation of azopolymer in multi-layered nanocomposites resulting in the enhanced chain rigidity and restricted the segmental mobility. The chain rigidity was also attributed to better interaction between the filler and polymer chains increasing the glass transition temperature. In this way, the thermal stability of new nanocomposites was enhanced relative to the reported materials [34].

Thermal stability was also investigated in terms of the initial degradation temperature (T_0), 10 % weight loss (T_{10}), maximum decomposition temperature (T_{max}) and char residue at 600 °C using TGA. According to the literature, degradation of NDs usually starts at 100 °C and continue up to 550 °C. When NDs were heated up to 600 °C, only 5 % of weight loss was generally observed due to the oxidation of graphite and amorphous carbon (sp^3 phase) content. A total weight loss of 11.5 % was observed at 900 °C, above which all oxygenated groups were usually released [34, 35].

Figure 9 shows a comparison between the thermal stability of NF-NDs/PAP/PANi/PPy and F-NDs/PAP/PANi/PPy nanocomposites. Thermogram of NF-NDs/PAP/PANi/PPy showed single stage decomposition starting at 444 °C and continuing up to 550 °C. Major weight loss was observed in the range of 444–559 °C. At this stage, polymer backbone was completely broken down and heavier products were disintegrated into smaller fragments and gaseous by products. NF-NDs/PAP/PANi/PPy exhibited char yield of 58 % at 600 °C. On the other hand, F-NDs/PAP/PANi/PPy showed T_0 of 459 °C, T_{10} at 489 °C, T_{max}

Table 2 Thermal analyses data of nanocomposites

Sample code	T_g (°C)	T_0 (°C)	T_{10} (°C)	T_{max} (°C)	Char yield (600 °C) (%)
NF-NDs/PANi/PPy/PTh	99	433	459	549	56
F-NDs/PANi/PPy/PTh	105	436	471	555	57
NF-NDs/PAP/PANi/PPy	109	444	483	559	58
F-NDs/PAP/PANi/PPy	118	459	489	567	59

T_g Glass transition temperature, T_0 initial decomposition temperature, T_{10} temperature for 10 % weight loss, T_{max} maximum decomposition temperature

around 567 °C and char yield of 59 %. NDs/PANi/PPy/PTh nanocomposite also showed single stage decomposition (Fig. 10). NF-NDs/PANi/PPy/PTh had T_0 of 433 °C, T_{10} at 459 °C and T_{max} at 549 °C. In contrast, F-NDs/PANi/PPy/PTh exhibited higher thermal degradation temperature as $T_0 = 436$ °C, $T_{10} = 471$ °C and $T_{max} = 555$ °C. On the whole, F-NDs/PANi/PPy/PTh and F-NDs/PAP/PANi/PPy based on functionalized nanodiamonds showed higher values in thermal properties and char residue.

XRD analysis

Final characteristics of the materials synthesized were studied using XRD analysis in the region $2\theta = 5°$–$50°$ at room temperature. The XRD scans of nanodiamonds and nanocomposites are presented in Fig. 11. The purified nanodiamond displayed peaks with 2θ values of 42.01°, 43.13° and 48.99° due to three-dimensional detonation nanodiamond structures. The diffractogram of functionalized nanodiamonds showed sharp peak at $2\theta = 43.46°$ depicting that the nanodiamond particulates were functionalized without altering the nanofiller crystalline structure. The characteristic peaks of NF-NDs/PANi/PPy/PTh were observed around $2\theta = 43.47°$. While F-NDs/PANi/PPy/PTh nanocomposite depicted diffraction peaks at 25.02° and 43.86°. The pattern of NF-NDs/PAP/PANi/PPy revealed three peaks at $2\theta = 17.22°$, 25.08° and 27.72°. Whereas, a broad peak appeared at $2\theta = 26.92°$ for F-NDs/PAP/PANi/PPy. For pure PANi, diffraction peaks have been observed at $2\theta = 20°$ and 25° due to the periodically arranged parallel and perpendicular polymer chain structures [36].

Electrical conductivity

Table 3 represents the electrical conductivity of hetero-aromatic NDs/PAP/PANi/PPy nanocomposites with

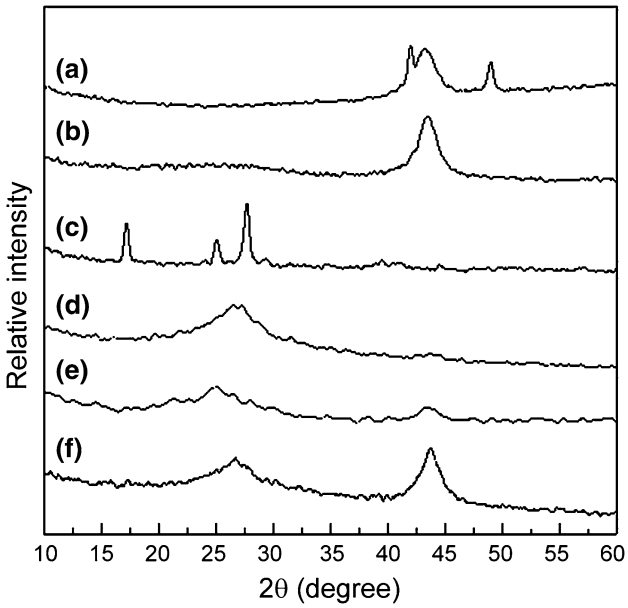

Fig. 11 XRD patterns of *a* purified nanodiamonds, *b* functionalized nanodiamonds, *c* NF- NDs/PANi/PPy/PTh, *d* F-NDs/PANi/PPy/PTh, *e* NF-NDs/PAP/PANi/PPy, and *f* F-NDs/PAP/PANi/PPy samples

Table 3 Conductivity measurements of nanocomposites

Sample code	Conductivity (Scm^{-1})
NF-NDs/PANi/PPy/PTh	2.9
F-NDs/PANi/PPy/PTh	3.7
NF-NDs/PAP/PANi/PPy	3.8
F-NDs/PAP/PANi/PPy	5.4

functionalized and non-functionalized filler. Multi-layered azo-, pyridine- and thiophene moieties were found to enhance the conductivity of nanocomposites. The conductivity of NF-NDs/PAP/PANi/PPy was 3.8 Scm^{-1} and was improved with functionalized filler in F-NDs/PAP/PANi/PPy as 5.4 Scm^{-1}. Whereas, NF-NDs/PANi/PPy/PTh and F-NDs/PANi/PPy/PTh nanocomposites had relatively lower values of 2.9 and 3.7 Scm^{-1}, respectively. Moreover, the increase in conductivity in this system was less significant.

Nanodiamonds, having high surface area and tunable surface structure, doped with conducting polymers showed significant enhancement in the electrical properties owing to the synergetic effects of layered conducting matrices and filler. Functionalized filler was found to enhance the electrical conductivity proficiently relative to non-functionalized filler due to better interaction with the matrices. Morphology comprising of fibrous matrix network with embedded functionalized nanodiamonds also assisted pathways for the transportation of electrons in functionalized nanocomposites. In the literature, nanodiamonds have

also been known to increase the electrical properties of the final composite material [37].

Conclusion

In this exploration, we have discussed the rational control of structural, thermal, morphological and electrical properties of nanocomposites through the surface modification of nanodiamonds as (a) introduction of functional groups and (b) in situ doping of various matrices over the filler surface. New layered polyaniline, polypyrrole, polythiophene and polyazopyridine nanocomposites filled with nanodiamond were obtained through facile synthetic strategy (in situ route). In particular, four types of nanocomposites were studied, i.e., non-functionalized and functionalized ND-based layered PAP/PANi/PPy and non-functionalized and functionalized ND-based layered PANi/PPy/PTh nanocomposites. Thermal and electrical properties of the nanodiamond composites comprising of nanodiamonds dispersed on polymeric fibers were considered. The addition of functionalized nanodiamonds to multi-polymer matrix enhanced the thermal stability and render the nanocomposite heat resistant at low filler concentration in contrast to NF-NDs containing systems. Functionalized nanodiamond-based hybrids also showed slight enhancement in the glass transition temperature of nanocomposites relative to non-functionalized systems. Newly prepared high-performance nanocomposites may be potentially applicable in Li-ion battery components, microelectronics and several energy-related industries.

References

1. Kausar A, Hussain ST (2014) Azo-polymer based hybrids reinforced with carbon nanotubes and silver nanoparticles: solution and melt processing. Int J Polym Mater 63:207–221
2. Zhai YJ, Wang ZC, Huang W, Huang JJ, Wang YY, Zhao YQ (2011) Improved mechanical properties of epoxy reinforced by low content nanodiamond powder. Mater Sci Eng A 528:7295–7300
3. Krueger A (2008) New carbon materials: biological applications of functionalized nanodiamond materials. Chem Eur J 14:1382–1390
4. Baidakova M, Vul A (2007) New prospects and frontiers of nanodiamond clusters. J Phys D Appl Phys 40:6300–6311
5. Koshcheev AP (2009) Thermodesorption mass spectrometry in the light of solution of the problem of certification and unification of the surface properties of detonation nano-diamonds. Russ J Gen Chem 79:2033–2044
6. Kulakova I (2004) Surface chemistry of nanodiamonds. Phys Solid State 46:636–643
7. Gopalakrishnan K, Elango M, Ramesh C, Thamilselvan M (2013) Catalytic-assisted synthesis, characterization and low frequency AC conduction of nanostructured conducting polyaniline. Iran Polym J 22:43–52
8. Jayamurgan P, Ponnuswamy V, Ashokan S, Mahalingam T (2013) The effect of dopant on structural, thermal and morphological properties of DBSA-doped polypyrrole. Iran Polym J 22:219–225
9. Channu VSR, Holze R, Rambabu B, Kalluru RR (2012) Synthesis and characterization of PANI nanostructures for supercapacitors and photoluminescence. Iran Polym J 21:457–462
10. Kruger A, Liang Y, Jarre G, Stegk J (2006) Surface functionalization of detonation diamond suitable for biological applications. J Mater Chem 16:2322–2328
11. Kruger A (2008) The structure and reactivity of nanoscale diamond. J Mater Chem 18:1485–1492
12. Chehrazi E, Qazvini NT (2013) Nanoconfined segmental dynamics in miscible polymer blend nanocomposites: the influence of the geometry of nanoparticles. Iran Polym J 22:613–622
13. Kausar A, Hussain ST (2013) Processing and properties of new heteroaromatic Schiff-base poly(sulfone-ester)s and their blends. Iran Polym J 22:175–185
14. Duan J, Shao S, Li Y, Wang L, Jiang P, Liu B (2012) Polylactide/graphite nanosheets/MWCNTs nanocomposites with enhanced mechanical, thermal and electrical properties. Iran Polym J 21:109–120
15. Afzal AB, Akhtar MJ (2012) Effects of silver nanoparticles on thermal properties of DBSA-doped polyaniline/PVC blends. Iran Polym J 21:489–496
16. Nistor MT, Vasile C (2013) TG/FTIR/MS study on the influence of nanoparticles content upon the thermal decomposition of starch/poly(vinyl alcohol) montmorillonite nanocomposites. Iran Polym J 22:519–536
17. Alaei MH, Mahajan P, Brieu M, Kondo D, Rizvi SJA, Kumar S, Bhatnagar N (2013) Effect of particle size on thermomechanical properties of particulate polymer composite. Iran Polym J 22:853–863
18. Puzyr AP, Baron AV, Purtov KV, Bortnikov EV, Skobelev NN, Mogilnaya OA, Bondar VS (2007) Nanodiamonds with novel properties: a biological study. Diam Relat Mater 16:2124–2128
19. Liu Y, Gu Z, Margrave JL, Khabashesku VN (2004) Functionalization of nanoscale diamond powder: fluoro-, alkyl-, amino-, and amino acid-nanodiamond derivatives. Chem Mater 16:3924–3930
20. Dolmatov VY (2001) Detonation synthesis ultradispersed diamonds: properties and applications. Russ Chem Rev 70:607–626
21. Kim H, Abdala AA, Macosko CW (2010) Graphene/polymer nanocomposites. Macromolecules 43:6515–6530
22. Sharp KG (1998) Inorganic/organic hybrid materials. Adv Mater 10:1243–1248
23. Fujiyama-Novak JH, Cakmak M (2008) Nanoparticle-induced radial structural gradients in melt-spun polypropylene/PP-*g*-MA Fibers. Macromolecules 41:6444–6452
24. Potts JR, Dreyer DR, Bielawski CW, Ruoff RS (2011) Graphene-based polymer nanocomposites. Polymer 52:5–25
25. Kuilla T, Bhadra S, Yao D, Kim NH, Bose S, Lee JH (2010) Recent advances in graphene based polymer composites. Prog Polym Sci 35:1350–1375
26. Winey KI, Vaia RA (2007) Polymer nanocomposites. MRS Bull 32:314–319
27. Yang S, Leong KF, Du Z, Chua CK (2001) The design of scaffolds for use in tissue engineering. Part I. Traditional factors. Tissue Eng 7:679–689
28. Zhang J, Qiu T, Ren S, Yuan H, He L, Li X (2012) Simple synthesis of polypyrrole–polystyrene hybrid hollow spheres. Mater Chem Phys 134:1072–1078
29. Ravichandran S, Nagarajan S, Kokil A, Ponrathnam T, Bouldin RM, Bruno FF, Nagarajan R (2012) Micellar nanoreactors for

hematin catalyzed synthesis of electrically conducting polypyrrole. Langmuir 28:13380–13386
30. Libo L, Jiajia W, Peixia Y, Shaowen G, Heng W, Xiuchun Y, Xuwei M, Shuo Y, Baohua W (2013) Preparation and characterization of gel polymer electrolytes containing *N*-butyl-*N*-methylpyrrolidinium bis(trifluoromethanesulfonyl) imide ionic liquid for lithium ion batteries. Electrochim Acta 88:147–156
31. Scrosati B (1998) Conducting polymers: advanced materials for new design, rechargeable lithium batteries. Polym Int 47:50–55
32. Osipov VY, Aleksenskiy AE, Shames AI, Panich AM, Shestakov MS, Vul AY (2011) Conducting polymers: advanced materials for new design, rechargeable lithium batteries. Diam Relat Mater 20:1234–1238
33. Mitev D, Dimitrova R, Spassova M, Minchev C, Stavrev S (2007) Surface peculiarities of detonation nanodiamonds in dependence of fabrication and purification methods. Diam Relat Mater 16:776–780
34. Morimune S, Kotera M, Nishino T, Goto K, Hata K (2011) Poly(vinyl alcohol) nanocomposites with nanodiamond. Macromolecules 44:4415–4421
35. Cataldo F, Koscheev AP (2003) Study on the action of ozone and on the thermal stability of nanodiamond. Fuller Nanotub Car N 11:201–218
36. Chaudhari HK, Kelkar DS (1997) Investigation of structure and electrical conductivity in doped polyaniline. Polym Int 42:380–384
37. Mochalin VM, Shenderova O, Ho D, Gogotsi Y (2012) The properties and applications of nanodiamonds. Nat Nanotech 7:11–23